PHYSICAL REVIEW B VOLUME 33, NUMBER 8 15 APRIL 1986

Structural transitions and metallization in compressed solid argon

A. K. McMahan
Lawrence Livermore National Laboratory, University of California, Livermore, California 94550
(Received 24 December 1985)

Total-energy calculations are reported for compressed solid Ar which suggest that the observed 1-atm fcc phase should transform to an hcp structure prior to metallization, and it in turn should transform to a bcc structure at pressures above metallization. It is argued that this structural sequence follows from the effects of hybridization between the l valence band and the $l+1$ conduction band as the gap narrows and closes, and that all rare-gas solids are likely to undergo an hcp→bcc transition with metallization occurring near, if not within, the range of hcp stability. The lower-pressure fcc→hcp transition in insulating Ar should occur below 230 GPa.

I. INTRODUCTION

There has been continuing interest in the metallization of compressed rare-gas solids since the early estimates of Herzfeld.[1] As the required pressure may vary with crystal structure, calculations for He (Ref. 2) and Xe (Refs. 3 and 4) have sought to determine the stable structure at metallization. In both cases crystallographic phase transitions were predicted in the vicinity of metallization; however, the question of whether or not the decreasing gap had actually driven these transitions was not addressed.

The present paper reports linear muffin-tin orbital calculations of the zero-temperature total energy differences between the fcc, hcp, and bcc structures of solid Ar. The structural transitions implied by these differences are listed in Table I, and the metallization volumes for the three structures, in Table II. These results suggest that the observed 1-atm fcc phase should transform to an hcp structure prior to metallization, and it should transform to a bcc phase at pressures above metallization. Both transitions are closely related to the onset of metallic conductivity. It is argued here that they are caused by the growing effects of hybridization between the $l+1$ conduction band and the l valence band as the insulating gap separating these bands decreases and then closes.

Combined with the previous work on He (Ref. 2) and Xe (Refs. 3 and 4), these calculations for Ar suggest that the rare-gas solids may follow a generalized structural sequence of cp→hcp→bcc, with metallization occurring near, if not within, the hcp interval. At low pressures the fcc and hcp structures are nearly degenerate in energy, which makes calculation of the observed low-pressure phases very difficult.[5] The present paper makes no attempt to deal with this problem, and designates the initial phase as simply close packed (cp). The point made here, and signified by cp→hcp, is that under significant compression this near degeneracy is broken in favor of the hcp structure due to the hybridization mechanism just mentioned.

Argon was chosen for the present work in part because of a recent suggestion that it might provide an alternate pressure standard for high-pressure diamond anvil cell measurements.[6] It would be important for such an application to consider possible structural transitions in the standard, as for example the fcc→hcp transition predicted here for Ar. Due to the exceedingly small hcp-fcc energy difference at low pressures, only an upper bound of ~230 GPa (2.3 Mbar) can be placed on this transition. Only above this pressure does the hcp-fcc difference become significantly larger than the uncertainties in the present calculations, clearly establishing hcp as more stable than the fcc structure observed at 1 atm. While this is within the 300 GPa range over which solid Ar is recommended[6] as a pressure standard, the differences in equation of state between the two structures are found to be sufficiently small so as not to compromise the desired application.

In the remainder of this paper the linear muffin-tin orbital (LMTO) calculations are described in Sec. II and the hybridization mechanism in Sec. III. Discussion of these results and conclusions are presented in Sec. IV.

TABLE I. Predicted structural transitions in compressed solid Ar. The volume, pressure, and percentage volume change are specified for each transition. Volume is relative to $V_0=37.45$ Å^3/atom. For the fcc→hcp entry, these results constitute only an upper (lower) bound on the transition pressure (volume).

Transition	V/V_0	P (GPa)	ΔV (%)
fcc→hcp	>0.25	<230	<0.1
hcp→bcc	0.148	970	0.7
bcc→fcc	0.103	2200	1.2

TABLE II. Metallization volumes and pressures for the fcc, hcp, and bcc structures of solid Ar. Volume is relative to $V_0=37.45$ Å^3/atom.

Structure	V/V_0	P (GPa)
fcc	0.186	550
hcp	0.204	430
bcc	0.223	330

II. LMTO CALCULATIONS

The LMTO method has been described in detail elsewhere.[7,8] The present calculations were nonrelativistic, used the von Barth—Hedin exchange-correlation potential,[9] and included Andersen's combined-correction term.[7,8] The metallization volumes and pressures in Table II were obtained from self-consistent calculations for the fcc, hcp, and bcc structures in which the $3s$ and $3p$ valence bands were sampled with 89, 80, and 140 points per irreducible wedge of the respective Brillouin zones. Angular momentum components of s,p,d,f character were retained. Core states were included in a self-consistent atomic manner.

The LMTO zero-temperature structural energy differences, relative to the fcc structure, are presented in Fig. 1 as a function of reduced volume V/V_0, where $V_0=37.45$ Å^3/atom is the observed[10] 1-atm $T=0$ volume of the fcc solid. These results were obtained using the force theorem,[11] providing more accurate differences than would be obtained from the separate self-consistent calculations just mentioned. In this approach, the total energy differences are given by differences in one-electron eigenvalue sums obtained using the same (in this case the self-consistent fcc) set of one-electron potentials for each of the three structures. Only the valence eigenvalues are involved, eliminating numerical uncertainties which can arise from large core contributions to all-electron total energies. Such calculations are also less expensive, permitting more dense sampling of the Brillouin zone than would otherwise be practical. The force theorem has been numerically tested for other third-period elements[12] and has proved remarkably successful in previous LMTO structural calculations.[13] It also requires an electrostatic Madelung contribution to the structural energy differences.[11] Although quite small, this contribution is included here by means of the muffin-tin or Ewald correction.[14]

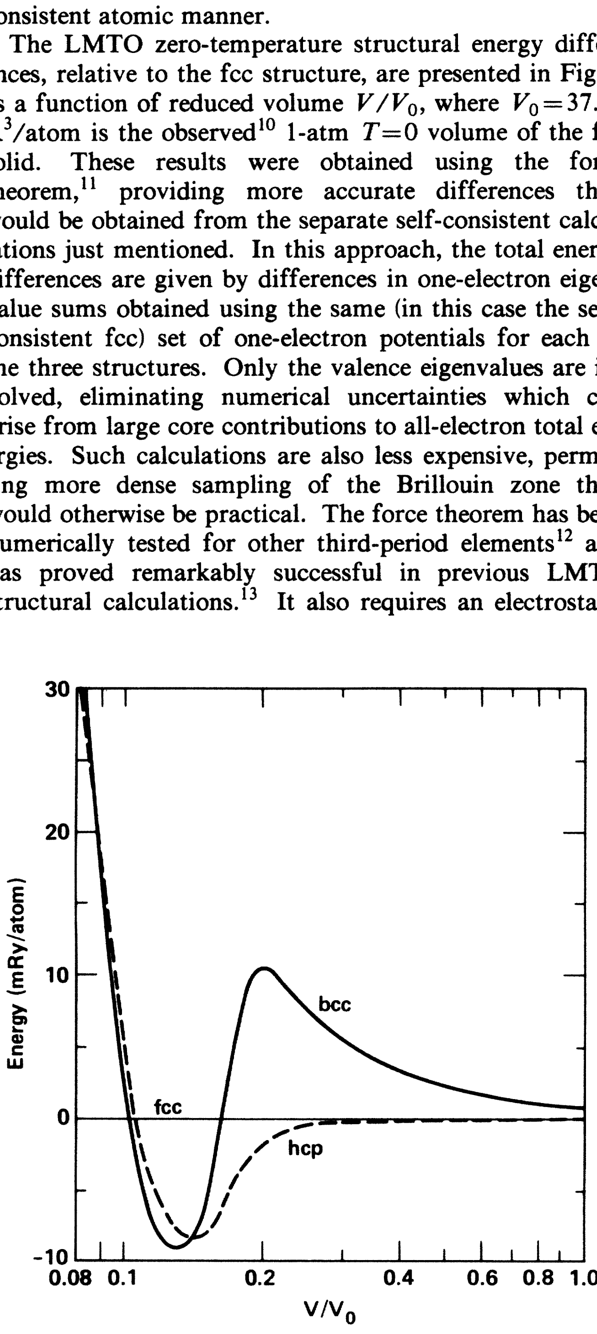

FIG. 1. LMTO calculated relative total energies of the fcc, hcp, and bcc structures of solid Ar as a function or reduced volume V/V_0.

The one-electron eigenvalue sums used in the force theorem calculations for the $3s$ and $3p$ valence electrons were obtained with 240, 150, and 285 points in the irreducible wedges of the fcc, hcp, and bcc Brillouin zones, respectively. Much coarser sampling is adequate in the insulating regions. These sampling densities were chosen to also yield convergence in the metallic regions, where a further approximate doubling of these densities resulted in change of the structural energy differences by less than 0.5 mRy/atom. Test calculations with the $2s$ and $2p$ electrons included as bands showed negligible contribution to the structural energy differences from these electrons over the range plotted in Fig. 1.

Components through f character were retained in the angular momentum basis used in calculating the results shown in Fig. 1. By far the greatest sensitivity to basis was found in the bcc-fcc curve for $V/V_0<0.18$. Its minimum near $V/V_0\sim0.13$ in Fig. 1, for example, has been lowered by nearly 17 mRy/atom by the inclusion of f components.[15] Selected tests with the basis further augmented to include g components indicated shifts an order of magnitude smaller, but not entirely negligible in this region. For this reason, calculations including g components were carried out in the vicinity of the transitions to determine the transition volumes cited in Table I. They are within 5% of values predicted by the s-f basis results shown in Fig. 1.

Separate panels were used for each of the nonoverlapping $3s$ and $3p$ bands in the range $V/V_0>0.25$. A single panel was used at smaller volumes when these bands overlapped. Tests were carried out in the region $V/V_0\leq0.25$ where this procedure might be most inaccurate, by using two overlapping panels. This required careful accounting to insure neither duplication nor omission of any eigenvalues. These tests gave the bcc-fcc peak near $V/V_0\sim0.2$ and the hcp-fcc curve in the same volume range to within 5% and 1%, respectively, of the single panel results shown in Fig. 1.

Linearization for each angular momentum component was carried out within each panel in the manner described by Skriver.[8] Two cases required special treatment: First, when separate panels were used for the $3s$ and $3p$ bands, $\langle \dot{\phi}^2_{\nu s}\rangle$ was set to 0 and $D_{\dot{\nu}s}>0$ for the s linearization in the upper, $3p$ panel. Second, $\varepsilon_{\nu f}$ was placed ~1.5 Ry above the f center of gravity for each panel in order to shift the $D_{\dot{\nu}f}$ branch of the f variational logarithmic derivative to a range which would not create f roots within the panel. Similar treatment was used for $\varepsilon_{\nu g}$. These adjustments eliminate the possibility of unphysical roots which might otherwise occur in certain easily identifiable circumstances, as discussed in detail in Ref. 8.

The bcc-fcc and hcp-fcc pressure differences ΔP at fixed volume were determined by numerical differentiation of the calculated structural energy differences. The bulk modulus B for the fcc phase was also determined by numerical differentiation of the fcc pressures mentioned earlier. Volume changes at the transitions were then obtained from $\Delta V/V=\Delta P/B_{\text{fcc}}$. They are so small, as seen in Table I, that no attempt was made to locate the boundaries of the two-phase regions. Except for the first entry, the transition volumes listed in Table I are those volumes at which the total energy curves cross, which lie within the two-phase regions. For volumes $V/V_0 < 0.25$ the present hcp-fcc energy difference is larger than the ~ 0.5 mRy/atom numerical uncertainty in these structural energy differences, indicating definite stability of the hcp structure. The transition from the observed 1-atm stable fcc structure to hcp should therefore occur at larger volumes or pressures (possibly much) less than 230 GPa.

III. CANONICAL BANDS AND HYBRIDIZATION

Some insight into the cp→hcp→bcc sequence suggested by Fig. 1 is provided by Andersen's canonical band theory along with the leading hybridization corrections to this theory.[7,8] The relevant equations are reviewed in the Appendix, and have been previously used to discuss the closely related problem of core contributions to the structural energy differences in highly compressed alkali metals.[16]

Within the atomic-phase approximation underlying the LMTO method, the one-electron eigenvalues ε may be approximated[7,8] in the absence of hybridization by

$$\varepsilon_{li}^{(0)}(\mathbf{k}) = C_l + \frac{1}{\mu_l S^2} \frac{\mathscr{S}_{li}(\mathbf{k})}{1-\gamma_l \mathscr{S}_{li}(\mathbf{k})} \ . \tag{1}$$

Here, the canonical bands $\mathscr{S}_{li}(\mathbf{k})$ depend only on $\mathbf{k}$ vector, angular momentum l, band index i, and crystal structure. They generate unhybridized bands for specific materials when centered about C_l, scaled in width according to the band mass μ_l, and distorted according to the parameter γ_l. All three of these (positive) potential parameters are material-dependent and Wigner-Seitz radius S-dependent, but structure independent.

Differences in Madelung energy between the structures considered here are small, so the force theorem[11] gives the total energy differences as just those between one-electron eigenvalue sums. Since averages $\langle \mathscr{S}_{li}(\mathbf{k}) \rangle = 0$ for full l bands, the leading contribution to the unhybridized structural energy difference $\Delta E^{(0)}$ is

$$\Delta E^{(0)} \sim \frac{\gamma_l}{\mu_l S^2} \Delta \langle [\mathscr{S}_{li}(\mathbf{k})]^2 \rangle \propto \frac{\gamma_l}{\mu_l S^2} \Delta (W_l^2) \ , \tag{2}$$

i.e., proportional to the difference in canonical bandwidth W_l squared. This is just the difference in Born-Mayer repulsion[17] between different structures, as those with smaller near-neighbor distances generally have larger bandwidths.

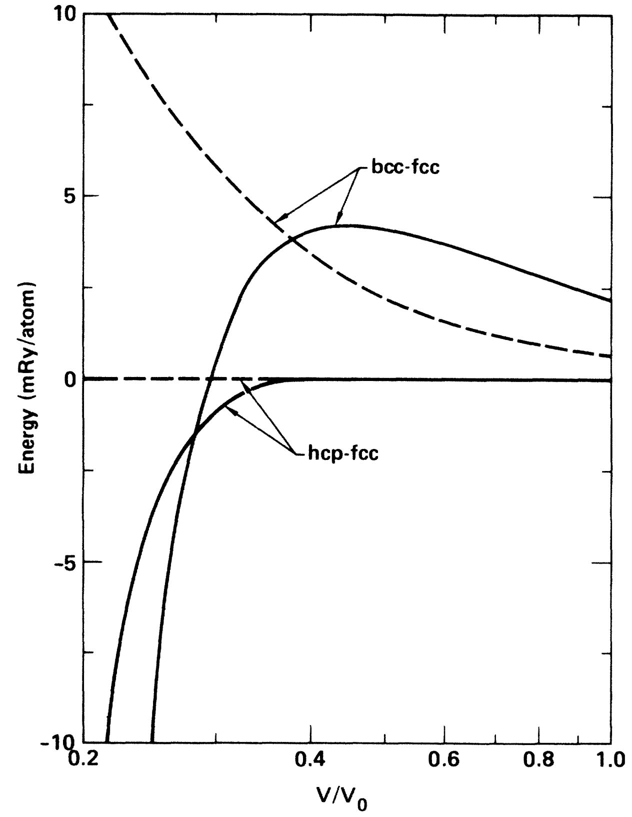

FIG. 2. Model calculation of the $3p$ contribution to the hcp-fcc and bcc-fcc total energy differences in solid Ar. The dashed curves are unhybridized results based on Eq. (1) of the text, and they show the effects of Born-Mayer repulsion. The solid curves include the leading hybridization corrections to the one-electron eigenvalues given by Eq. (3).

The dashed curves in Fig. 2 show bcc-fcc and hcp-fcc differences $\Delta E^{(0)}$ for the $3p$ band of Ar. Differences between sums over the eigenvalues given by Eq. (1) were used, in order to provide more accurate results than would be obtained from the leading term Eq. (2). It is not surprising to see the bcc structure unstable relative to the two close-packed phases, given its smaller near-neighbor distance. With identical first- and second-neighbor distances, the hcp and fcc structures have nearly degenerate energies in these unhybridized calculations, although the fcc structure is slightly favored. There are no phase transitions here.

It requires the effects of hybridization to introduce the sequence of phase transitions indicated in Fig. 1. As derived in the Appendix, the leading correction to Eq. (1), designated $\varepsilon_{li}^{(2)}(\mathbf{k})$, is second order in the hybridization matrix elements $\mathscr{S}_{li,\lambda j}(\mathbf{k})$, which couple angular momentum l with λ, for band indices i and j, respectively:

$$\varepsilon_{li}^{(2)}(\mathbf{k}) = \frac{1}{\mu_l S^2} \left[\frac{\varepsilon_{li}^{(0)} - V_l}{C_l - V_l} \right]^2 \sum_{\lambda,j}{}' \frac{1}{\mu_\lambda S^2} \left[\frac{\varepsilon_{\lambda j}^{(0)} - V_\lambda}{C_\lambda - V_\lambda} \right]^2 \frac{\varepsilon_{li}^{(0)} - V_\lambda}{\varepsilon_{\lambda j}^{(0)} - V_\lambda} \frac{|\mathscr{S}_{li,\lambda j}(\mathbf{k})|^2}{\varepsilon_{li}^{(0)} - \varepsilon_{\lambda j}^{(0)}} \ . \tag{3}$$

The sum excludes $\lambda = l$. The parameters in this equation are illustrated for Ar in Fig. 3. The eigenvalues $\varepsilon_{li}^{(0)}(\mathbf{k})$ lie in the shaded l bands centered about the dashed lines C_l with width related to the band masses μ_l. The actual boundaries here in Fig. 3 (solid lines) are energies where the logarithmic derivatives $D_l = 0$ and ∞.

Equation (3) clearly shows the repulsion between levels which is associated with the concept of hybridization. Whether, for example, the 3s levels are pushed down by the 3p band above (see Fig. 3) or pushed up by the 2p band below (not shown) is determined by which of the p bands is closer. In Andersen's canonical band theory this boundary is established by the parameters (dotted lines) V_l defined as the energies for which $D_l = l$ (V_s coincides with the bottom of the s bands).[7,8] Thus the factor $\varepsilon_{li}^{(0)} - V_\lambda$ in Eq. (3) is quite important. It is interesting to note that levels such as the 3p near $V/V_0 = 1$, which lie *below* V_{3d} and V_{4f} (dotted lines labeled d and f), are pushed *up* by pd and pf hybridization just as if there were 2d and 3f bands below.

The solid lines in Fig. 2 show the bcc-fcc and hcp-fcc structural energy differences for the 3p band obtained using the sum of Eqs. (1) and (3) for the one-electron eigenvalues. The downward turn of both the bcc-fcc and hcp-fcc curves for $V/V_0 < 0.4$ is due to hybridization with the 3d band (the 4f as well in the first case). These effects are small at larger volumes due to the large 3p-3d separation [the quotient $\varepsilon_{li}^{(0)} - \varepsilon_{\lambda j}^{(0)}$ in Eq. (3)], and kept small for decreasing volume until after V_{3d} has cut through most of the 3p band (the factor $\varepsilon_{li}^{(0)} - V_{3d}$).

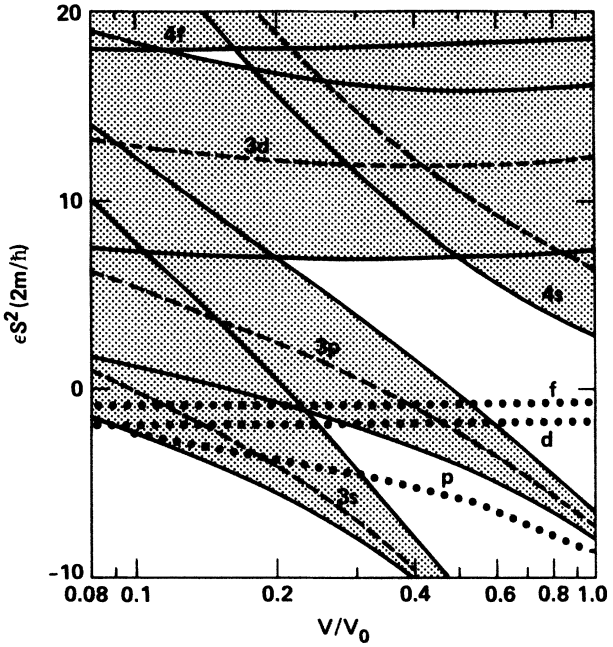

FIG. 3. Energy parameters ε entering Eqs. (1) and (3) of the text, as a function of reduced volume. The dimensionless product $\varepsilon S^2 2m/\hbar^2$ is shown. The unhybridized eigenvalues $\varepsilon_{li}^{(0)}$ lie in the shaded regions which are bounded by the solid lines, centered about the C_l (dashed curves), and of width $\propto \mu_l^{-1}$. The dotted lines are the energies V_l.

The 3p-band model calculations in Fig. 2 predict an fcc→hcp→bcc sequence in qualitative agreement with Fig. 1, however, with the transitions at larger volumes. Addition of the 3s-band contributions to Fig. 2 only slightly shifts these volumes. A more important source of the difference is inclusion of the combined correction[7,8] in the full LMTO calculations, which does shift the transitions to smaller volumes as well as making the bcc-fcc maximum more sharply peaked. It corrects for the fact that the Hamiltonian and overlap matrix elements should be evaluated over the Wigner-Seitz polyhedron, and not sphere, as is the case in the atomic-sphere approximation on which the formalism in the Appendix is based.

The largest difference between Figs. 1 and 2 is simply the breakdown of the perturbation treatment used to obtain Eq. (3) as the bands move close together. The solid lines in Fig. 2 are in fact in close agreement with LMTO results for the 3p band carried out without the combined correction for $V/V_0 > 0.35$. However, as the 3p and 3d levels approach one another, Eq. (3) diverges, exaggerating the pd-hybridization effect due to the energy denominators $(\varepsilon_{pi}^{(0)} - \varepsilon_{dj}^{(0)})$. The model used to obtain Fig. 2 also omits the effects of 3p-band depopulation following metallization, which are responsible for the return to fcc stability in Fig. 1 for $V/V_0 < 0.1$.

Results for the 3s-band contribution to the structural energy differences as obtained by Eqs. (1) and (3) are qualitatively the same as those for the 3p band in Fig. 2, except that the important hybridization effect driving the bcc-fcc and hcp-fcc curves downward is due to the nearby 3p band, and not the more distant 3d band. This is entirely consistent with the fact that LMTO calculations for He also gave an fcc→hcp→bcc transition in the vicinity of metallization.[2]

IV. DISCUSSION

Both the present calculation for Ar and earlier LMTO work[2] on He predict cp→hcp→bcc structural sequences for these compressed rare gas solids, with metallization occurring during the interval of hcp stability. Perturbation theory correctly predicts the ultimate high-pressure structure of He to be bcc;[2,18] however, the theory breaks down at lower pressures where the 1s shell is fully intact.[2] Were the hcp structure omitted, both He and Ar would undergo fcc→bcc transitions near (although just after) metallization, in qualitative agreement with work[3,4] for Xe which did not include this structure. The combined work for He, Ar, and Xe thus appears to be in substantial qualitative agreement, suggesting that the cp→hcp→bcc sequence found here for Ar may well be a generalized structural sequence for all of the rare-gas solids.

The theoretical prediction of any structural sequence is of course subject to the caveat that the set of structures considered is complete. In this regard it might be noted that the rare-gas cores dominate the structural energy differences of highly compressed alkali metals, and that Cs is indeed predicted to undergo an hcp→bcc transition at a compression slightly beyond where the 5p core and 5d valence bands begin to overlap.[16] For Rb and K, on the other hand, this sequence is interrupted by small stability regions of Sm-type and of both Sm-type and dhcp (double hcp) structures, respectively.[16] While it is beyond the scope of this paper to consider these structures for Ar, the possibility of intermediate stability for these more complex close-packed phases between the hcp and bcc phases suggested above for the rare-gas solids must be acknowledged.

Despite its lack of p valence electrons, He is expected[2] to undergo the same hcp→bcc transition found here for Ar. The model calculations reported in Sec. III corroborate this behavior, and offer insight into the origin of the full cp→hcp→bcc sequence itself. They suggest that the transitions are driven by the effects of hybridization between an l valence band and an upper lying $l+1$ conduction or valence band. Whether $l=s$ or p, these hybridization shifts in the l valence band serve to favor bcc and hcp structures (in that order) over fcc as the gap between the l and the $l+1$ bands decreases. As this effect must first overcome the Born-Mayer repulsion penalty in the bcc case, the hcp structure has an intermediate range of stability where this hybridization contribution dominates the energy difference between the two close-packed phases.

The hcp-fcc energy difference found here for Ar near $V/V_0=1$ is more than an order of magnitude smaller than the uncertainties in the present calculations. Only above ~230 GPa does this difference become sufficiently large to clearly establish high-pressure hcp stability. The anticipated fcc→hcp transition in Ar could occur well below this upper bound in pressure. While within the 300-GPa range over which solid Ar has been proposed for a standard,[6] the small volume change ($<0.1\%$) at the transition, and small equation of state differences ($<0.4\%$ in pressure at fixed volume) between the two close-packed phases should not compromise the use of Ar as a standard. In fact, the fcc→hcp transition might provide a convenient fixed point as part of the pressure calibration.

ACKNOWLEDGMENTS

This work was performed under the auspices of the U.S. Department of Energy by Lawrence Livermore National Laboratory under Contract No. W-7405-Eng-48.

APPENDIX

This appendix reviews the derivation of Andersen's "second-order" Hamiltonian,[7,8] followed by an expansion of this quantity to obtain Eqs. (1) and (3) of the text. The starting point is the secular equation for the one-electron eigenvalues ε,

$$\det[P_l(\varepsilon)\delta_{ll'}\delta_{mm'}-\mathscr{S}_{lm,l'm'}(\mathbf{k})]=0\ , \tag{A1}$$

which is formally common to both the Korringa-Kohn-Rostoker method[17] as well as the atomic-sphere approximation underlying the LMTO method.[7,8] In the latter case of interest here, the structure constants $\mathscr{S}_{lm,l'm'}(\mathbf{k})$ are energy independent, and

$$P_l(\varepsilon)=2(2l+1)[D_l(\varepsilon)+l+1]/[D_l(\varepsilon)-l]\ ,$$

where $D_l(\varepsilon)$ are logarithmic derivatives of the radial wave functions evaluated at the Wigner-Seitz sphere radius S.

An excellent fit to the functions $P_l(\varepsilon)$ may be obtained in the vicinity of the unhybridized l-band centers C_l, by the three-parameter (C_l,μ_l,γ_l) form

$$P_l(\varepsilon)\sim\frac{\mu_l S^2(\varepsilon-C_l)}{1+\gamma_l\mu_l S^2(\varepsilon-C_l)}\ . \tag{A2}$$

Given this expression for $P_l(\varepsilon)$, the eigenvalues of Eq. (A1) are then identically those of Andersen's second-order Hamiltonian

$$H=C+(\mu S^2)^{-1/2}\mathscr{S}(1-\gamma\mathscr{S})^{-1}(\mu S^2)^{-1/2}\ , \tag{A3}$$

where

$$C=[C_l\delta_{ll'}\delta_{mm'}],\ \ \mu=[\mu_l\delta_{ll'}\delta_{mm'}],\ \ \gamma=[\gamma_l\delta_{ll'}\delta_{mm'}]$$

are diagonal matrices in lm, and $\mathscr{S}$ is the $\mathbf{k}$-dependent structure constant matrix. The eigenvalues of Eq. (A3) are accurate to second order in $\varepsilon-C$, compared to those obtained from the exact expression for $P_l(\varepsilon)$, thence the reference to second-order Hamiltonian.

The unhybridized one-electron energies $\varepsilon_{li}^{(0)}$ given by Eq. (1) of the text are eigenvalues of

$$H_0=C+(\mu S^2)^{-1}\mathscr{S}_0(1-\gamma\mathscr{S}_0)^{-1}\ , \tag{A4}$$

where $\mathscr{S}_0$ is just $\mathscr{S}$ with all matrix elements coupling dissimilar l's set to zero. The eigenvalues $\mathscr{S}_{li}(\mathbf{k})$ (i is the band index) of $\mathscr{S}_0$ itself are Andersen's canonical bands.[7,8] In the remainder of this Appendix, all matrices will be considered in a basis within which $\mathscr{S}_0$ and thus H_0 are diagonal.

It is straightforward to expand H about H_0 in powers of the hybridization matrix $\mathscr{S}-\mathscr{S}_0=[\mathscr{S}_{li,\lambda j}(\mathbf{k})(1-\delta_{l\lambda})]$,

$$H=H_0+\Delta T\sum_{n=0}^{\infty}[(1-\gamma\mathscr{S}_0)\gamma\mu S^2\Delta T]^n\ , \tag{A5}$$

where

$$\Delta T=(\mu S^2)^{-1/2}(1-\gamma\mathscr{S}_0)^{-1}(\mathscr{S}-\mathscr{S}_0)\times(1-\gamma\mathscr{S}_0)^{-1}(\mu S^2)^{-1/2}\ . \tag{A6}$$

The leading correction $\varepsilon_{li}^{(2)}$ to the unhybridized eigenvalues $\varepsilon_{li}^{(0)}$ is quadratic in the hybridization matrix elements $\mathscr{S}_{li,\lambda j}(\mathbf{k})$, and is given by

$$\varepsilon_{li}^{(2)}=\frac{1}{\mu_l S^2(1-\gamma_l\mathscr{S}_{li})^2}\sum_{\lambda,j}{}'\frac{1}{\mu_\lambda S^2(1-\gamma_\lambda\mathscr{S}_{\lambda j})^2}\,|\mathscr{S}_{li,\lambda j}(\mathbf{k})|^2\left[\frac{1}{\varepsilon_{li}^{(0)}-\varepsilon_{\lambda j}^{(0)}}+\frac{1}{\varepsilon_{\lambda j}^{(0)}-C_\lambda+(\gamma_\lambda\mu_\lambda S^2)^{-1}}\right]\ , \tag{A7}$$

where the first (second) term in the large parentheses comes from a second- (first-) order perturbation treatment of the $n=0$ ($n=1$) term in Eq. (A5).

Equation (A7) may be put in the form given by Eq. (3) of the text using

$$\gamma_l \mu_l S^2 (C_l - V_l) = 1 \tag{A8}$$

and

$$1 - \gamma_l \mathscr{S}_{li} = \frac{C_l - V_l}{\varepsilon_{li}^{(0)} - V_l} \; . \tag{A9}$$

Equation (A8) is an approximation consistent with that of Eq. (A2), since V_l is defined to be the energy ε where $D_l(\varepsilon)=l$ and thus $P_l(\varepsilon)$ diverges. The parameters V_l define the boundaries between l bands of different principal quantum number and are crucial to the treatment of hybridization using Eq. (3). Thus it is best to choose γ_λ in Eq. (A7) such that Eq. (A8) yields an accurate value for V_λ, rather than to give an improved fit to the true $P_\lambda(\varepsilon)$ in the vicinity of the λ-band center C_λ.

---

[1] See discussion and references in M. Ross, Rep. Prog. Phys. **48**, 1 (1985) and A. Jayaraman, Rev. Mod. Phys. **55**, 65 (1983). Recent work on Ne is reported by J. Hama, Phys. Lett. **105A**, 303 (1984) and by J. C. Boettger, Phys. Rev. B (to be published).

[2] D. A. Young, A. K. McMahan, and M. Ross, Phys. Rev. B **24**, 5119 (1981).

[3] J. Hama and S. Matsui, Solid State Commun. **37**, 889 (1981).

[4] A. K. Ray, S. B. Trickey, and A. B. Kunz, Solid State Commun. **41**, 351 (1982).

[5] K. F. Niebel and J. A. Venables, in *Rare Gas Solids*, edited by M. L. Klein and J. A. Venables (Academic, London, 1976), Chap. 9.

[6] M. Ross, H. K. Mao, P. M. Bell, and J. A. Xu, in *Proceedings of the APS Topical Conference on Shock Waves in Condensed Matter—1985* (Plenum, New York, 1985).

[7] O. K. Andersen, Phys. Rev. B **12**, 3060 (1975); O. K. Andersen and O. Jepsen, Physica (Utrecht) **91B**, 317 (1977); O. K. Andersen, in *The Electronic Structure of Complex Systems*, edited by P. Phariseau (Plenum, New York, 1983).

[8] H. L. Skriver, *The LMTO Method* (Springer, Berlin, 1984).

[9] U. von Barth and L. Hedin, J. Phys. C **5**, 1629 (1972).

[10] J. Donohue, *The Structure of the Elements* (Wiley, New York, 1974), p. 27.

[11] A. R. Mackintosh and O. K. Andersen, in *Electrons at the Fermi Surface*, edited by M. Springford (Cambridge University Press, Cambridge, 1980).

[12] A. K. McMahan and J. A. Moriarty, Phys. Rev. B **27**, 3235 (1983).

[13] H. L. Skriver, Phys. Rev. B **31**, 1909 (1985).

[14] E. Esposito, A. E. Carlsson, D. D. Ling, H. Ehrenreich, and C. D. Gelatt, Jr., Philos. Mag. A **41**, 251 (1980); D. Glötzel and O. K. Andersen (unpublished).

[15] Reference 6 cited preliminary work by the present author in which only s,p,d components were included in the angular momentum basis and the hcp structure constants were not fully converged, erroneously indicating continued fcc stability in compressed Ar.

[16] A. K. McMahan, Phys. Rev. B **29**, 5982 (1984). Equation (2) of this reference is Eq. (3) of the present work with the further approximation $\varepsilon_{\lambda j}^{(0)} \sim C_\lambda$.

[17] See, e.g., N. W. Ashcroft and N. D. Mermin, *Solid State Physics* (Holt, Rinehard and Winston, Philadelphia, 1976).

[18] H. Niki, H. Nagara, H. Miyagi, and T. Nakamura, Phys. Lett. **79A**, 428 (1980).